An Interferer-Tolerant CMOS Code-Domain Receiver Based on N-Path Filters

Abhishek Agrawal, *Member, IEEE*, and Arun Natarajan, *Member, IEEE*

***Abstract*— This paper extends N-path filtering to the code domain by proposing code-modulated local oscillator signals. A correlator-based perspective of N-path mixer receiver (RX) is presented to demonstrate interferer-rejection and desired signal reception in a code-domain N-path RX. Pairs of Walsh-function-based codes are proposed for modulating desired RX and known interferers [such as self-interference (SI) from transmitter (TX)] to achieve high interferer rejection. An N-path architecture for concurrent reception of two code-modulated signals is also presented. A 0.3–1.4-GHz 65-nm CMOS implementation achieves 35-dB gain for desired signals and concurrently receives two RX signals while rejecting mismatched spreading codes at RF input. The proposed TX SI mitigation approach results in 38.5-dB rejection for −11.8 dBm 1.46-Mb/s quadrature phase-shift keying (QPSK) modulated SI at the RX input. The RX achieves 23.7-dBm output referred 1dB gain compression (OP1dB) for in-band SI, while consuming ∼35 mW and occupies 0.31 mm^2. Such code-domain selection/rejection can be used in conjunction with other N-path filtering schemes for signal selection/rejection based on a combination of spatial, spectral, and code-domain properties.**

***Index Terms*— CMDA, CMOS, code domain, interferer rejection, N-path filter, receiver, self-interference (SI) suppression, self-interferer, Walsh function.**

I. Introduction

THE demand for higher network capacity with available spectrum has motivated efforts to further increase spectrum reuse by targeting higher cellular densification, simultaneous transmit-and-receive (STAR), and dynamic spectrum access/carrier aggregation [1], [2]. Such networks require interferer-tolerant receivers (RX) capable of handling blockers from other transmitters (TX) as well as self-interference (SI) from its TX. N-path mixer-based RX promise high blocker tolerance since they enable tunable local oscillator (LO)-defined RF filtering. Bandpass and bandstop N-path filters have been analyzed and demonstrated [3]–[6]. N-path filtering combining bandpass and bandstop filters has also been demonstrated with up to ∼13-dBm blocker tolerance [7], [8]. Spectral selectivity of N-path RX has been extended to spatio-spectral selectivity by receiving [9] or rejecting [10], [11] an input signal at certain frequency and angle of incidence. The feasibility of concurrently rejecting multiple interferers based on spatio-spectral properties has been demonstrated in [11]. Notably, non-reciprocal networks have also been demonstrated using such N-path mixers, achieving integrated circulators [12]. In this case, the N-path network targets cancellation of the TX SI at the RX input achieving full-duplex (FD) operation [2], [13]. N-path based FD transceivers (TRX) using baseband TX canceling have been demonstrated in [14]. In summary, prior N-path mixer based approaches have focused on signal filtering in the spatial/frequency domain and also demonstrated shared antenna interfaces with TX SI cancellation (SIC).

In this paper, N-path filter operation is extended to the code domain to demonstrate the feasibility of selecting/rejecting signals based on their code-domain properties [15]. The proposed N-path mixer RX architecture rejects blockers modulated with other codes *at the RF input*, leading to higher blocker tolerance. A possible application for STAR TRX with code-domain TX SIC is demonstrated. In addition, the feasibility of achieving concurrent reception of two code-modulated signals using N-path networks is also shown. Such code-domain selection/rejection can be potentially applied to communication and radar systems operating on code-modulated signals and can be used in conjunction with other N-path schemes for signal selection/rejection based on a combination of spatial, spectral, and code-domain properties [11].

This paper is organized as follows. Section II provides a brief introduction to interferer tolerance in the context of code-domain signal processing. Section III extends N-path mixer architecture to the code domain and presents approaches for interferer and self-interferer rejection. Section IV describes an implementation using the proposed approach in 65-nm CMOS, and measurement results are detailed in Section V. Conclusions and future work extending LO sequence-mixing concepts are described in Section VI.

II. In-Band Interferers in a Code-Domain Receiver

Code-domain systems where each signal is spread using codes that are orthogonal to each other enable co-existence of multiple signals in the same frequency band. Such code-domain techniques are extensively used in code division multiple access (CDMA) communication and radar systems, leveraging correlation and processing gain as summarized below.

The interference and desired signals incident on a typical code-domain RX are shown in Fig. 1. The desired signal is a narrowband signal, with bandwidth BW_S that has been spread using a code PN_1, with a chip rate of B_C. As shown in Fig. 1, the RX is subject to out-of-band blockers as well as in-band narrowband and wideband interferers. The RX frontend must

Manuscript received August 28, 2017; revised October 25, 2017; accepted November 13, 2017. Date of publication February 15, 2018; date of current version April 23, 2018. This paper was approved by Guest Editor Osama Shanaa. This work was supported by the DARPA Arrays at Commercial Timescales program. *(Corresponding author: Arun Natarajan.)*

The authors are with the School of Electrical Engineering and Computer Science, Oregon State University, Corvallis, OR 97331 USA (e-mail: agrawala@eecs.oregonstate.edu; nataraja@eecs.oregonstate.edu).

Color versions of one or more of the figures in this paper are available online at http://ieeexplore.ieee.org.

Digital Object Identifier 10.1109/JSSC.2017.2777821

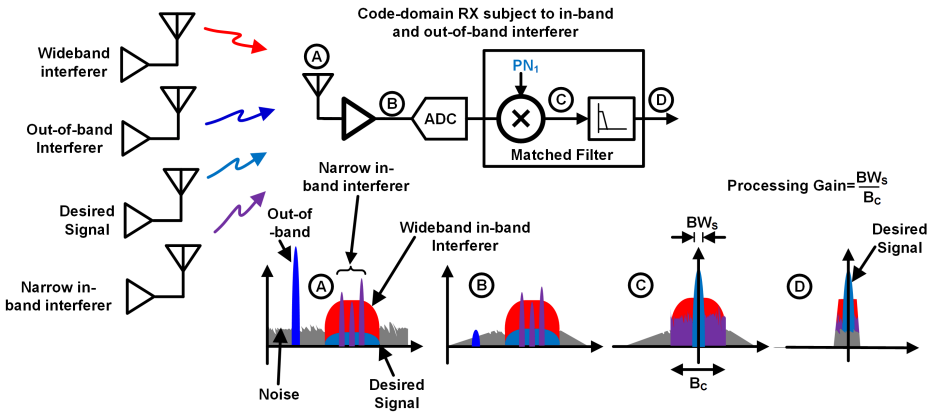

Fig. 1. Narrowband and wideband interferer rejection and desired signal reception with processing gain in a code-domain receiver.

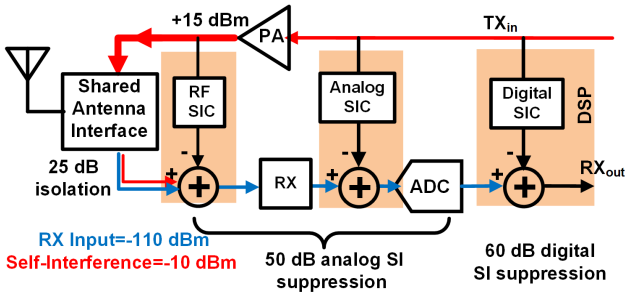

Fig. 2. RF, analog, and digital SIC in a STAR TRX.

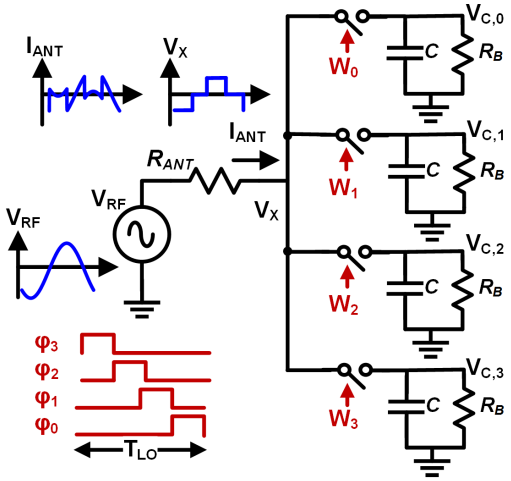

Fig. 3. N-path mixer-based RX with NOP LO signals.

filter out-of-band blockers while in-band interferer suppression is achieved digitally in the code domain. Following digitization, multiplication by the despreading code PN_1 in the RX results in recovery of the desired narrow-band signal. The despreading code also results in the power of the narrow in-band interferer (at node C in Fig. 1) getting distributed over the bandwidth, B_C. Subsequently filtering (node D in Fig. 1) thus attenuates interferer power by M where $M = (B_C/BW_S)$. Similarly, a wideband interferer is also multiplied by the despreading code. This also results in a wideband signal that is distributed over the spreading bandwidth, and hence the interferer is attenuated by a factor M by the filtering at node D. Importantly, if the narrowband or wideband interferer signal strength is high enough, non-linearities resulting from RX saturation limit processing gain.

Such strong interferers can easily arise in the case of STAR TRX as shown in Fig. 2. In this case, the TX SI couples into the RX either through leakage in the shared antenna interface (circulator or duplexer) or through antenna coupling in the case of separate TX and RX antennas. In typical CDMA systems with frequency-domain duplexing, the TX leakage is frequency filtered to provide SI rejection. However, there is increasing interest in systems operating in the same frequency band, such as FD communication as well as radar systems. Assuming ~15-dBm TX power and 25-dB TX–RX isolation, the SI power at RX input is −10 dBm. Achieving 10 dB of input-referred signal-to-interference-plus-noise ratio (SINR) for a −110-dBm RX signal requires 110-dB SIC [16]. Analog-to-digital converter resolution limits digital SIC to ~60 dB, which implies that the analog front-end must provide ~50 dB SIC. It is desirable to achieve low-noise SIC early in the signal chain to enable amplification of the desired signal without additional noise from the cancellation circuitry.

In the following, we present an N-path RF correlation-based approach to attenuate out-of-band blockers and in-band interferers spread with different codes. The proposed code-modulated LO approach can also be used to reject TX SI by using orthogonal sequences to modulate TX and desired RX signals. This approach provides ~35-dB SIC at RF and must be accompanied by analog and digital SIC for further SI attenuation in practical systems.

III. Code-Domain N-Path Mixer-Based Receiver

A. N-Path Mixer as Correlation-Based RX

The N-path passive mixer driven by non-overlapping pulse (NOP) LO is shown in Fig. 3. Assuming that the RF input signal $V_{RF}(t) = V_{BB}(t)\cos(2\pi f_0 t + \theta)$, the baseband

capacitor voltages $V_{C,k}(t)$ are given by

$$V_{C,k}(t_0) = \frac{1}{C}\int_0^{t_0}\left(I_{\rm ANT}(t)W_k - \frac{V_{C,k}(t)}{R_B}\right)dt \tag{1}$$

where

$$I_{\rm ANT}(t) = \frac{V_{\rm RF}(t) - \sum_{j=0}^{j=3} V_{C,j}(t)W_j}{R_A}. \tag{2}$$

$R_A = R_{\rm ANT} + R_{\rm SW}$, and $W_j = \varphi_K$ (NOPs shown in Fig. 3). Since the pulses are non-overlapping

$$\frac{1}{T}\int_0^T \varphi_i(t)\varphi_j(t)dt = \begin{cases}\frac{1}{N}, & \text{if } i = j\\ 0, & \text{if } i \neq j\end{cases} \tag{3}$$

where $N = 4$ in the four-path filter in Fig. 3. Using (2) and (3) in (1), and assuming that $V_{C,k}(t)$ is constant over $T_{\rm LO}$, it can be shown that a Fourier transform of (1) leads to

$$V_{C,k}(\omega) = \frac{j\omega C R_{\rm eff}}{1 + j\omega C R_{\rm eff}} \times \mathcal{F}\left(\frac{1}{R_A C}\int_0^{t_0} V_{\rm RF}(t)W_k dt\right) \tag{4}$$

where $R_{\rm eff} = NR_A \parallel R_B$. The capacitor voltages from (4) are identical to that derived in [3]. Signals at frequencies close to $f_{\rm LO}$ harmonics are received at the baseband output while out-of-band signals are filtered since the $(V_{\rm RF}(t) \cdot W_k)$ term averages to zero.

Hence, the orthogonality of the NOP leads to the voltage across the capacitor depending on the correlation of input signal and corresponding NOP in (4) or *the N-path RX can be considered as a correlator where each capacitor stores the correlation between the input signal and the LO sequence applied to the switches*. Since this topology correlates the current through the switches with the LO sequence in (1), the correlation is affected by charge sharing that occurs if two of the switches placed in parallel are enabled at the same time [17]. This restricts the set of LO sequences that can be applied to the switches. Such restrictions can be avoided in approaches that correlate RF voltage with switches, as described in [11].

B. Code-Domain N-Path Passive-Mixer-Based RX

In the following, we assume a code-modulated desired RF input, $V_{\rm RF}(t)$, that is given by:

$$V_{\rm RF}(t) = (V_{\rm BB}(t) \cdot {\rm PN}_{R1}) \cdot \cos(2\pi f_0 t + \theta) \tag{5}$$

where $V_{\rm BB}(t)$ is the desired signal, with bandwidth, BW_S, modulated with a code, PN_{R1}, with a chip rate, $C_R = 1/T_C$.

We consider the case when $V_{\rm RF}(t)$ is the signal incident on the code-modulated RX input along with a narrowband interferer, $V_J(t)$, as shown in Fig. 4. The LO signal applied to each switch is generated by multiplying the NOP with period, $T_{\rm LO} = 1/f_{\rm LO}$, with a pseudo-noise sequence, $PN_{\rm LO}$, as shown in Fig. 5.

An LO signal modulated with $PN_{\rm LO}$ code requires signals with (1,−1) polarity, as opposed to the (0, 1) NOP LO. This is emulated by using the scheme in Fig. 5: when code $PN_{\rm LO}(t)$ is 1, the NOP, φ_K, is directly applied to the switches and when

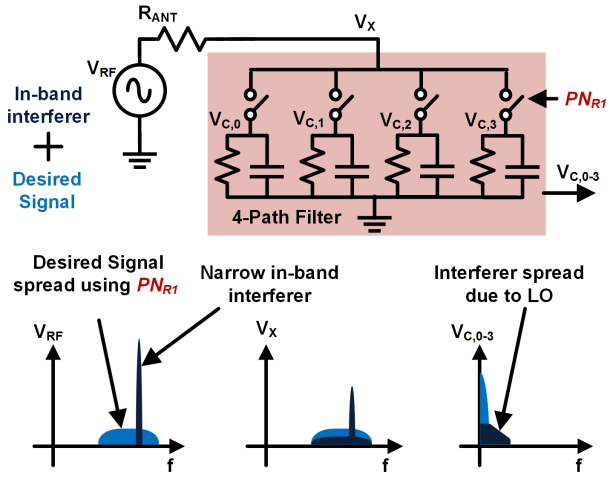

Fig. 4. Code-domain RX using N-path mixers with code-modulated LO.

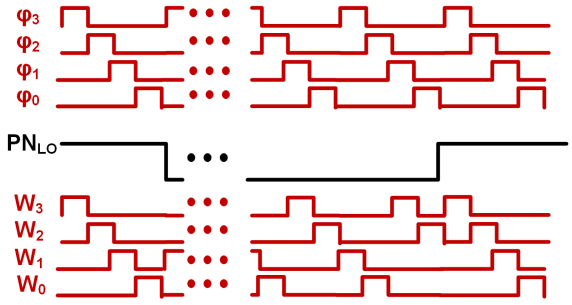

Fig. 5. LO generation by modulating NOP LO pulses with PN codes.

the code $PN_{\rm LO}(t)$ is −1, the NOP is shifted by 180^o phase and applied to the switches. This is feasible since the codes are running at much slower rate compared with RF frequency. Therefore, the LO sequences, W_K, are given by

$$W_k = \begin{cases}\varphi_k(t) & \text{for } {\rm PN}_{\rm LO}(t) = 1\\ \varphi_k(t + \pi/\omega_0) & \text{for } {\rm PN}_{\rm LO}(t) = -1.\end{cases} \tag{6}$$

Hence, the baseband capacitor voltages are given by

$$V_{C,k}(\omega) = \frac{j\omega C R_{\rm eff}}{1 + j\omega C R_{\rm eff}} \times \mathcal{F}\left(\frac{1}{R_A C}\int_0^{t_0} V_{\rm BB}(t)\ {\rm PN}_{R1}\cos(2\pi f_0 t + \theta)\ {\rm PN}_{\rm LO}\varphi_k dt\right). \tag{7}$$

If $V_{\rm BB}(t)PN_{R1}PN_{\rm LO}$ varies slowly with respect to $T_{\rm LO}$, (7) can be approximated as

$$V_{C,k}(\omega) = \frac{j\omega C R_{\rm eff}}{1 + j\omega C R_{\rm eff}} \times \mathcal{F}\left(\frac{c_k}{R_A C}\int_0^{t_0} V_{\rm BB}(t)\ {\rm PN}_{R1}\ {\rm PN}_{\rm LO} dt\right)$$

where

$$c_k = \frac{1}{T_{\rm LO}}\int_0^{T_{\rm LO}} \cos(2\pi f_0 t + \theta)\varphi_k dt. \tag{8}$$

Thus, $V_{C,k}(t)$ depends upon cross correlation between $PN_{\rm LO}$ and PN_{R1}. Assuming $PN_{\rm LO} = PN_{R1}$ and perfect synchronization between the PN codes ($PN_{\rm LO} \cdot PN_{R1} = 1$), (7) reduces to (4) and despreading of the desired signal occurs on the baseband capacitors. On the other hand, a low cross correlation between $PN_{\rm LO}$ and PN_{R1} or a carrier frequency that is not close to the harmonics of $f_{\rm LO}$ results in an attenuated baseband signal, providing interferer rejection.

The N-path code-domain RX hence *provides code-domain and spectral-domain filtering*. Out-of-band interferers are attenuated similar to the N-path RX with NOP LO in Fig. 3. The code-modulated LO also distributes in-band narrowband interferer power over a wider bandwidth, leading to interferer attenuation due to the low-pass filtering at capacitor output. Similarly, for wideband interferer modulated with a code different from $PN_{\rm LO}$, low-pass filtering reduces interferer power, improving overall signal-to-interferer ratio.

Similar to N-path RX operating in the frequency domain [3], impedance translation occurs for the code-domain N-path RX. For the desired coded signal, the baseband voltage across capacitor is upconverted and observed at V_X (Fig. 4), which provides impedance matching at antenna whereas for an unknown interferer, $V_{C,k}(t)$ is small, translating to a low RF input impedance. Thus, *code mismatch leads to reflected power at RF input*.

The PN code family for modulating LO can be selected based on auto-correlation for synchronization and cross correlation for interferer rejection properties [18], [19]. Based on (7), interferer rejection is dependent upon the cross correlation of $PN_{\rm LO}$ and the code used to modulate the interferer. Widely known Gold sequences [20] and Kasami sequences [21] with bounded cross correlation between sequence pair can be used to reject interferers [18], [19]. However, for known interferers, such as TX SI, orthogonal codes with zero cross correlation such as Walsh codes can be used to modulate the interferer and desired signals for high interferer rejection. In the following, the application of the code-domain RX for SI rejection is demonstrated by using orthogonal codes based on a combination of PN and Walsh sequences.

C. Walsh Functions/PN Sequences for SI Cancellation

The code-domain selectivity of the RX makes it possible to address STAR SIC challenges outlined in Section II for a code-domain TRX (Fig. 2). In this case, selection of Walsh Function sequences (WF-seq)-based codes for TX and RX spreading is shown to provide high level of SI rejection. WF-seq are orthogonal sequences well suited for digital synthesis [22]. Notably, a PN sequence multiplied by a WF-seq is also a PN sequence. An example of third-order WF-seq with eight sequences [wal(0)–wal(7)] is shown in Fig. 6. Following the notation in [22], the sequences are named sal (sine Walsh) and cal (cosine Walsh) to note the similarity to Fourier basis functions [22]. In the following, we consider two PN sequences, $PN_{\rm WF,1}$ and $PN_{\rm WF,2}$, where:

$$\mathrm{PN}_{\rm WF,1} = \mathrm{PN}_1 \cdot \mathrm{sal}(1); \quad \mathrm{PN}_{\rm WF,2} = \mathrm{PN}_1 \cdot \mathrm{cal}(3) \tag{9}$$

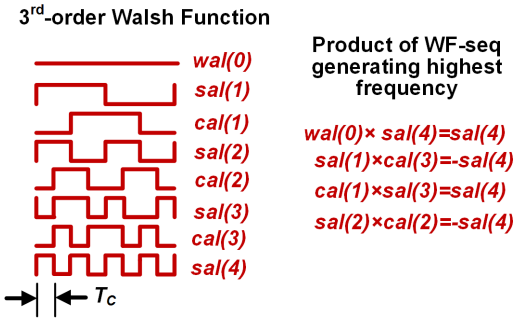

Fig. 6. Third-order WF-seq.

where sal(1) and cal(3) are shown in Fig. 6 and PN_1 is a pseudo-noise sequence with chip rate, $C = 1/T_C$.

The desired input signal, $V_{\rm RX}(t)$, is assumed to be spread using $PN_{\rm WF,2}$ and the TX signal, $V_{\rm TX}(t)$, is assumed to be spread using $PN_{\rm WF,1}$ such that

$$V_{\rm RX}(t) = (V_{\rm BB,RX} \cdot \mathrm{PN}_{\rm WF,2}) \cos(2\pi f_0 t + \Theta_1) \tag{10}$$

$$V_{\rm TX}(t) = (V_{\rm BB,TX} \cdot \mathrm{PN}_{\rm WF,1}) \cos(2\pi f_0 t + \Theta_2). \tag{11}$$

If the LO sequence applied to the mixers, W_J, is generated using $PN_{\rm WF,2}$ as described in (6) and assuming synchronization between the input RX signal, the LO code, and the TX spreading sequence

$$V_{\rm BB,RX} \cdot \mathrm{PN}_{\rm WF,2} \cdot \mathrm{PN}_{\rm WF,2} = V_{\rm BB,RX} \tag{12}$$

$$V_{\rm BB,TX} \cdot \mathrm{PN}_{\rm WF,1}\mathrm{PN}_{\rm WF,2} = \mathrm{sal}(4) \cdot V_{\rm BB,TX}. \tag{13}$$

Applying (12) and (13) in (8) (with $PN_{\rm LO} = PN_{\rm WF,2}$, $PN_{R1} = PN_{\rm WF,2}$ for the RX and $PN_{R1} = PN_{\rm WF,1}$ for the TX SI), the SI and desired RX signal at the baseband output are given by

$$V_{C,k,\rm TXSI}(\omega) = \frac{j\omega C R_{\rm eff}}{1 + j\omega C R_{\rm eff}} \times \mathcal{F}\left(\frac{c_k}{R_A C}\int_0^{t_0} V_{\rm BB,TX}(t)\mathrm{sal}(4)dt\right) \tag{14}$$

$$V_{C,k,\rm RX}(\omega) = \frac{j\omega C R_{\rm eff}}{1 + j\omega C R_{\rm eff}} \times \mathcal{F}\left(\frac{c_k}{R_A C}\int_0^{t_0} V_{\rm BB,RX}(t)dt\right). \tag{15}$$

From (14), SI interaction with RX despreading code translates SI to higher (out-of-band) frequencies, enabling frequency filtering in the RX baseband. A simplified visualization is shown in Fig. 7 where the desired RX and TX SI are incident on the N-path RX with code-modulated LO. Ensuring that the LO code is orthogonal to the TX and the same as RX results in the desired signal getting correlated on the N-path capacitors. Importantly, the TX SI is translated to higher frequency at RX output due to the choice of TX and LO codes, and hence can be filtered. While (14) is analyzed for one combination of WF-seq, other WF-seq combinations (Fig. 6) lead to the same result, with higher order WF-seq providing higher number of pairs.

The analysis in (14) is verified with simulations shown in Fig. 8. The TX signal is assumed to be spread with

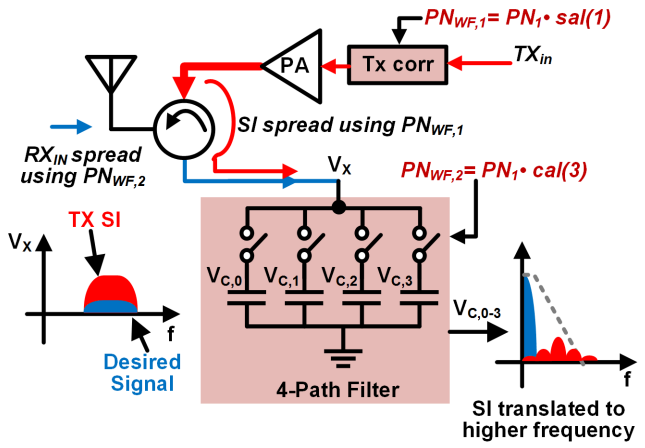

Fig. 7. SI frequency translation in code-domain RX with Walsh-function-based PN code pairs for the desired RX and TX signal.

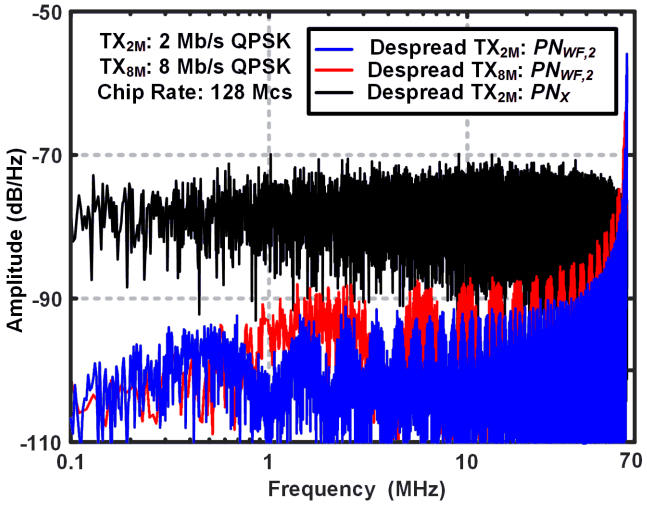

Fig. 8. Simulated SI at code-domain N-path RX output following despreading using PN code and WF-seq/PN code.

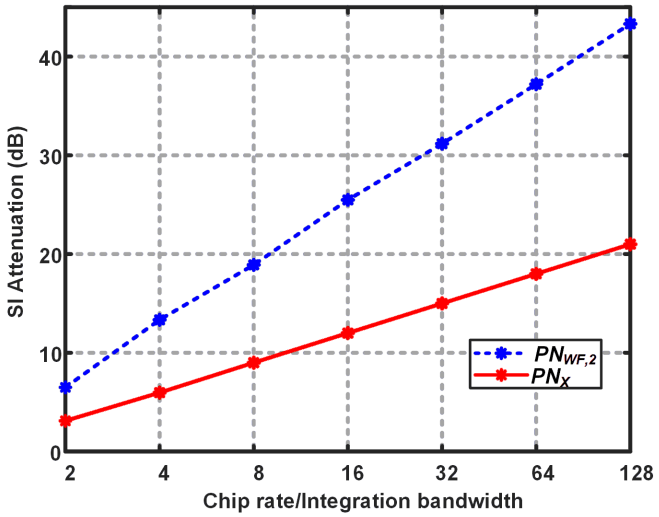

Fig. 9. Simulated SI attenuation across the ratio of chip rate and integration bandwidth.

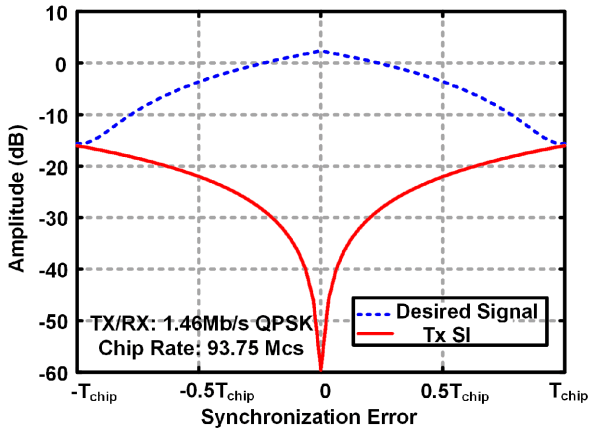

Fig. 10. Simulated SI rejection as a function of synchronization error.

code $PN_{\mathrm{WF},1}$ with a chip rate of 128 Mchips/s (Mcs). Two quaternary phase-shift keying (QPSK) TX symbol rates are considered: 1) 2 Mb/s (TX_{2M}) and 2) 8 Mb/s (TX_{8M}). An input power of 0 dBm is assumed for the SI. The SI for TX_{2M} is compared for two cases: 1) when the RX LO is modulated with $PN_{\mathrm{WF},2}$ and 2) with a randomly selected PN sequence, PN_X [generated using a different seed compared with PN_1 in (9)]. As expected from (14), the SI in the case of TX_{2M} is translated to higher frequencies at the baseband output with $PN_{\mathrm{WF},2}$ LO sequence compared with PN_X LO sequence. In both cases, the residual SI power is calculated by integrating the spectrum up to 1 MHz assuming an ideal brick-wall low-pass filter. Compared with 17.7-dB SI rejection with PN_X LO sequence, the orthogonal code, $PN_{\mathrm{WF},2}$, leads to 41.7-dB rejection, demonstrating 24-dB higher rejection. SI rejection achieved with code-modulated LO is a function of the ratio of the baseband integration bandwidth and chip rate. As shown in Fig. 8, a four times higher bandwidth for TX_{8M} leads to reduced SI rejection of 29.6 dB for TX_{8M} over the higher integration bandwidth of 4 MHz (assuming ideal brick-wall filter), when compared with the SI rejection for 1-MHz bandwidth.

Fig. 9 plots the simulated SI rejection across the ratio of chip rate and integration bandwidth, or processing gain. Higher SI rejection for a given bandwidth or a higher bandwidth for a given level of SI rejection can be achieved by increasing the chip rate. When the TX SI is despread using a randomly selected PN_X LO, the residue power spectrum is equally distributed over a bandwidth determined by chip rate. Therefore, doubling the processing gain leads to 3-dB reduction in the SI power. However, when the TX SI is despread with the orthogonal code, $PN_{\mathrm{WF},2}$, the SI at RX output is high-pass shaped. This results in 6-dB higher SI rejection for every doubling of processing gain.

The synchronization required between the TX and RX codes implies that the TX code must be aligned with the desired RX code using pilot signals, similar to a CDMA RX. MATLAB simulations, shown in Fig. 10, indicate 40-dB rejection with 5% timing error with respect to the chip period.

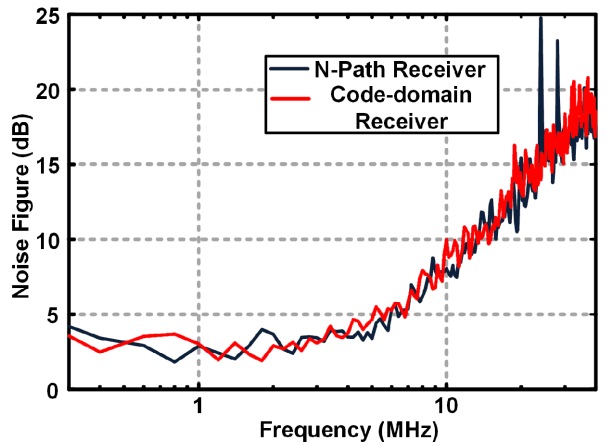

Fig. 11. Simulated RX NF with and without code modulation using Y-factor method.

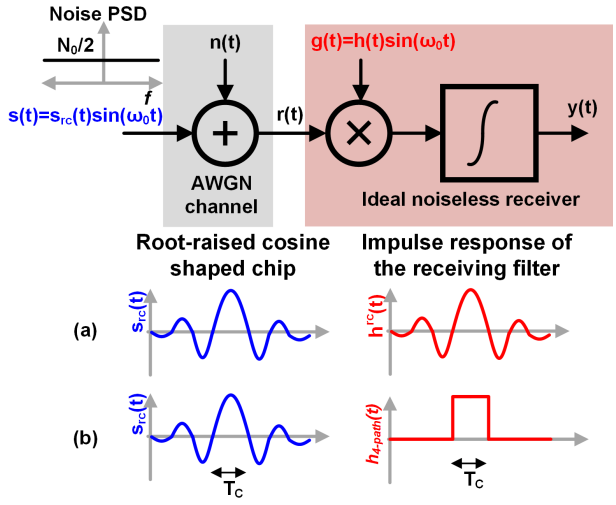

Fig. 12. NF degradation due to mismatch between waveform shaping of the chip and impulse response of the receiving filter. (a) Ideal matched filter implementation. (b) Filter that models the code-domain N-path RX.

D. RX Noise

The RX noise figure (NF) is simulated using the Y-factor method [23] by emulating hot and cold noise sources with 50-Ω impedance. Since the despread code is applied in the LO path, the RX NF does not degrade with the code-modulated LO as shown in Y-factor simulations of an N-path mixer RX with and without code-modulated LO (Fig. 11). However, despreading of the RX signal using a code-modulated LO does introduce noise due to sub-optimal filtering. The input RX signal bandwidth is limited in practice since the PN-coded signal is filtered using waveform shaping functions such as root-raised cosine filters prior to transmission. In the digital code-domain RX described in Fig. 1, the received signal can go through a matched filter with the same waveform shaping function, maximizing SNR [19].

A simplified RX diagram shown in Fig. 12 consists of an input signal $s(t)$ and the receiving filter with impulse response $g(t)$ in the presence of additive white Gaussian noise $n(t)$ from the channel. The energy of a chip with finite duration T can be expressed as

$$\varepsilon_s = \int_0^T s^2(t)dt. \tag{16}$$

Without loss of generality, if the signal $s(t)$ is normalized to have unit energy, the SNR of the received signal $y(t)$ at the output of the receiving filter can be calculated as

$$\frac{S}{N} = \frac{2}{N_0}\frac{\left[\int_0^T h(\tau)s(T-\tau)d\tau\right]^2}{\int_0^T h^2(t)dt} = \frac{2}{N_0}\frac{1}{F_d} \tag{17}$$

where, F_d denotes NF degradation due to mismatch between $s(t)$ and RX filter impulse response. For example, when a root-raised cosine filtered input signal [Fig. 12(a)] is passed thorough the RX filter with the same impulse response, the matched filtering does not degrade SNR and $F_d = 1$. However, in the code domain N-path RX, the RX filter impulse response is a pulse that degrades NF by 0.9 dB assuming root-raised cosine filtering of chip as shown in Fig. 12.

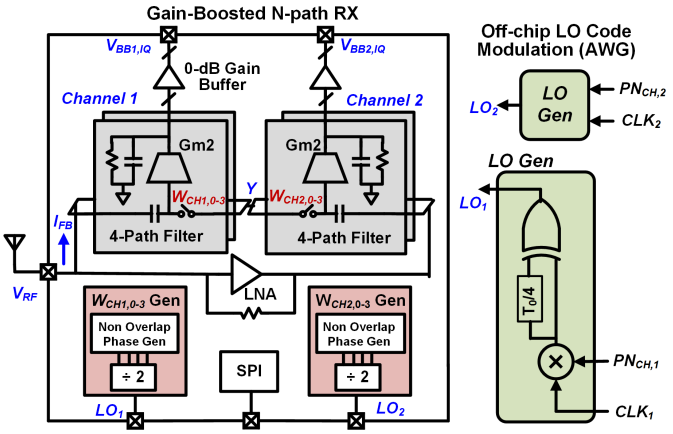

Fig. 13. Schematic of the gain-boosted N-path RX with two series N-path correlators in feedback path for concurrent reception of two signals.

IV. Proposed Code Domain Receiver in 65-nm CMOS

The proposed code-domain RX is demonstrated using a gain-boosted N-path RX [24] as shown in Fig. 13. The gain-boosted approach leads to lower NF; however, RX linearity is lower compared with passive mixer-first RX. In this paper, two correlators (N-path filters) are placed in series for concurrent reception of two signals. Since the same RF current, I_{FB}, passes through both N-path filters, the current can be used for concurrent correlation based on the analysis in (1). Considering operation in the frequency domain, if the LO switches in one correlator are clocked at f_1, the correlator presents a low impedance at other frequencies (ignoring parasitics). Additionally, if two correlators are placed in series, the current through them is the same. Hence, if the correlators, $CH1$ and $CH2$, are driven at two different frequencies, f_1 and f_2, the impedance at f_1 and f_2 is determined by the channels clocked at respective frequencies, enabling concurrent dual-frequency matching.

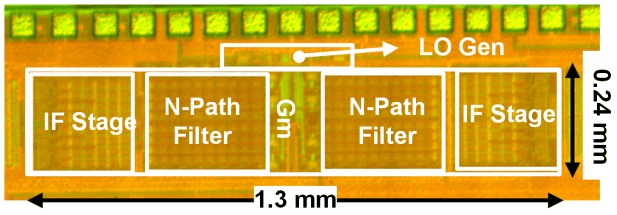

Fig. 14. Die photograph of the 65-nm CMOS gain-boosted N-path RX.

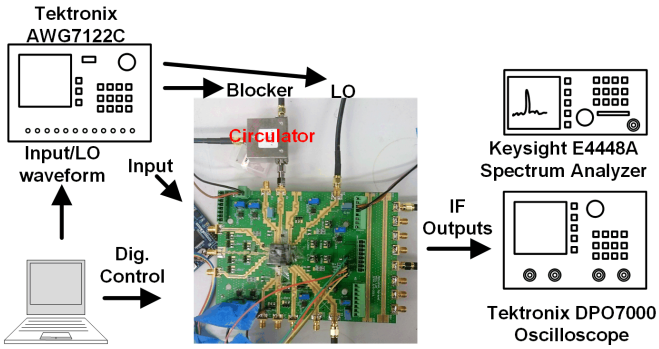

Fig. 15. Test setup for code-domain N-path RX using chip-on-board packaging.

In the proposed scheme, the LO switches in the two channels, $CH1$ and $CH2$, are driven at two different frequencies, f_1 and f_2, *and with different PN sequences,* PN_{CH1} *and* PN_{CH2}. Signals that are at the same frequency and have been spread using the same code as the frequency and codes for $CH1$ or $CH2$ see impedance matching at RF. Out-of-band signals or in-band signals spread with other codes lead to null voltages on the correlator capacitors. Therefore, the N-path RX presents a low impedance for such signals, leading to rejection at RX input. However, two series correlators in the feedback path increase the effective switch resistance, which impacts linearity. Rejection of undesired signals requires equivalent RF current to be sourced by the low noise amplifier (LNA) output. Higher resistance due to the two correlators in series leads to larger voltage swing at the LNA output for a given blocker level, degrading linearity. On the other hand, increasing the switch size increases the parasitics capacitance that shunts RF current to substrate degrading the high-frequency operation. In this design, a switch resistance of 15 Ω is selected to balance operation beyond 1 GHz with linearity.

The two four-path correlators are implemented in the feedback path as shown in Fig. 13 followed by a second IF stage and a buffer stage to drive 50-Ω load with 0-dB gain. The bandwidths of the N-path filter and second IF stage are 5 and 3.4 MHz, respectively.

NOP generation is accomplished using on-chip frequency dividers and logic gates. PN code-modulated off-chip LO is generated (shown in Fig. 13) using arbitrary waveform generator in this paper. Simulated power consumption of an on-chip LO code modulation scheme is < 1 mW in simulation. However, this does not power consumption of additional circuits required to provide fine delay control in the LO path for synchronization.

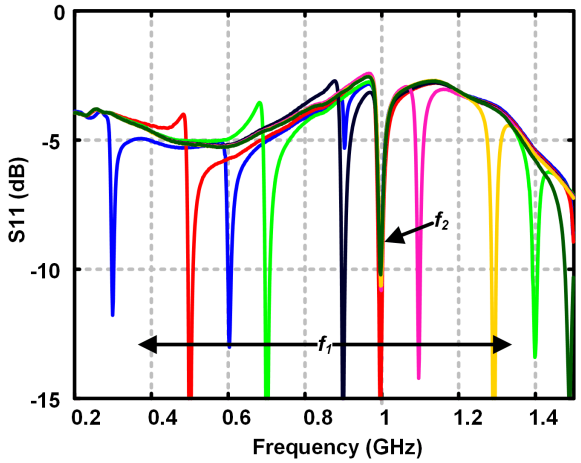

Fig. 16. Measured S11 with CH2 fixed at 1 GHz while CH1 is varied demonstrating concurrent dual-frequency matching.

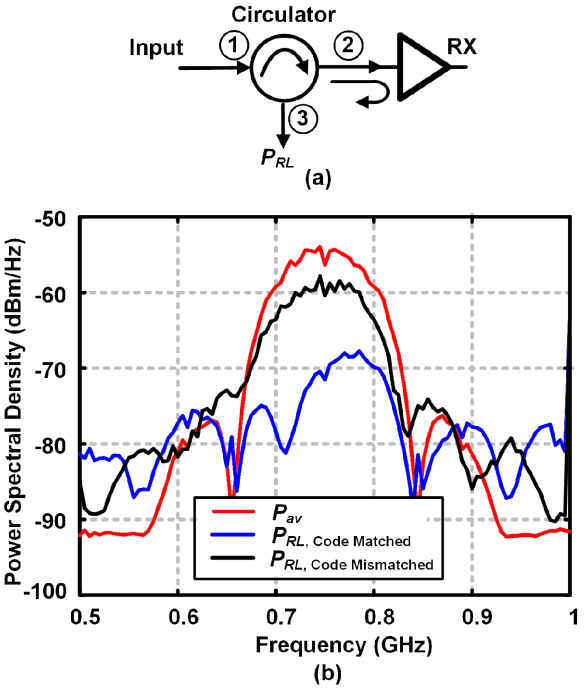

Fig. 17. (a) Code domain matching measurement setup. (b) Measured available and reflected power for matched and mismatch despreading codes.

V. Measured Performance

A. Small-Signal and Linearity Measurements

The RX occupies 0.31 mm^2 in a 65-nm CMOS technology as shown in Fig. 14. The chip-on-board packaging-based measurement setup is shown in Fig. 15. Fig. 16 shows the measured S11 when W_{CH1} and W_{CH2} are four-phase NOP without code modulation at two frequencies, f_1 and f_2. Frequency f_2 is held constant at 1 GHz while f_1 is varied from 300 MHz to 1.4 GHz. Concurrent LO tunable dual-frequency match is observed at f_1 and f_2 in Fig. 16.

A code domain matching measurement is performed using the circulator-based setup shown in Fig 17(a). The objective

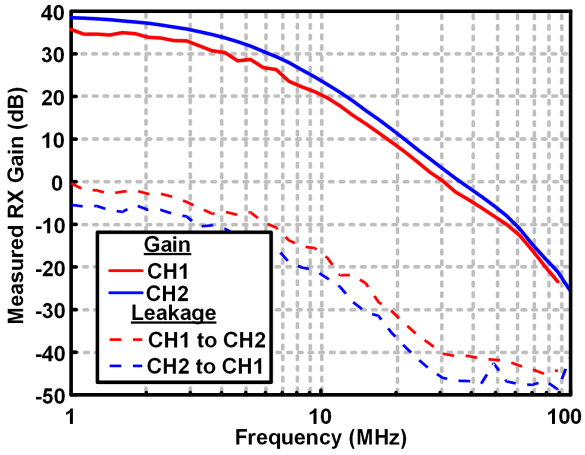

Fig. 18. Measured receiver gain and isolation between CH1 and CH2.

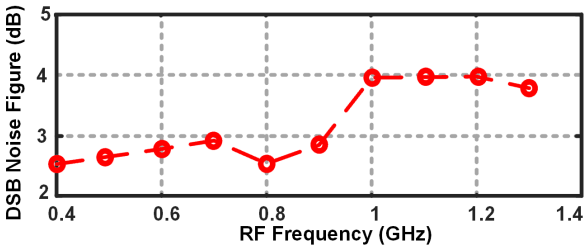

Fig. 19. Measured RX NF for CH1 across LO frequency.

of this measurement is to determine power reflected from RX input for a code-modulated input signal in order to evaluate RX input matching in the code domain. The reflected power at the RX input is measured at Port 3 of a circulator [Fig. 2(a)], where Port 1 is connected to the power source, and Port 2 is connected to the RX input. The reflected power is measured across different codes modulating the RX LO for a given code-modulated input signal. The measured spectrum of the available power at the RX (Port 2) is compared with the measured spectrum of the reflected power from the RX at Port 3 when the despreading code in the RX is the same and different from the spreading code for the input signal. A 10-dB higher reflected power at Port 3 is measured in Fig. 17(b) when the codes are mismatched compared with when the codes are matched, *demonstrating that code-mismatched signals are reflected at RF input.*

Fig. 18 shows the RX gain and the isolation between the channels CH1 and CH2. The concurrent measured gains at CH1 and CH2 are 35.5 dB (1-GHz RF input) and 38.5 dB (600-MHz RF input), respectively. Isolation between CH2 and CH1 is measured by measuring the CH1 output when the RF input frequency is close to the CH2 LO frequency. The measured isolation between the channels is ∼35dB as shown in Fig. 18. It should be noted that due to the reception of LO harmonics in N-path RX, the channel frequencies for concurrent reception cannot have a harmonic relationship. The measured RX NF across LO frequency from 0.3 to 1.4 GHz is shown in Fig. 19.

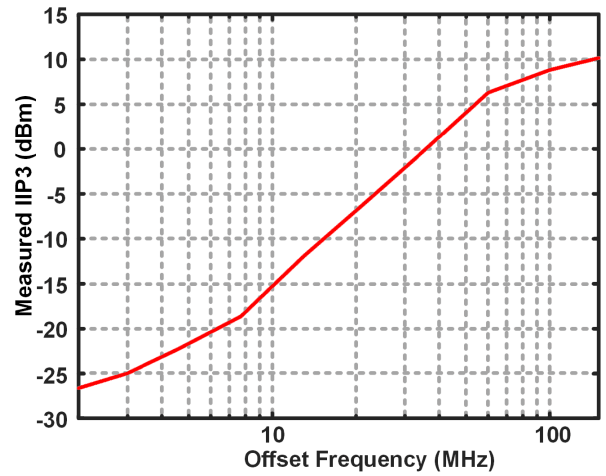

Fig. 20. Measured two-tone linearity across offset frequencies.

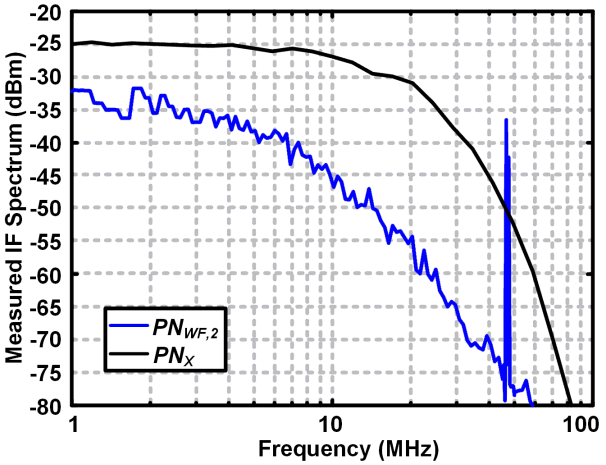

Fig. 21. Measured RX output spectrum for a two-tone TX input following spreading $\mathrm{PN}_{\mathrm{WF},1}$ and despreading with PN_X and $\mathrm{PN}_{\mathrm{WF},2}$.

The in-band IIP3 and out-of-band IIP3 of the RX are measured without code modulation. The measured in-band IIP3 of the receiver is −26 dBm as shown in Fig. 20. In conjunction with the 35.5-dB gain, this results in a + 9.5-dBm output-referred IP3 for in-band desired signals.

B. Interferer Rejection

As demonstrated in the measurements in Fig 17, the proposed approach leads to code-mismatched signals at RF input. Fig. 21 shows the RX output spectrum for two scenarios of code-modulated LO. In this measurement, a two-tone TX baseband signal at 0.5 and 1.5 MHz is used. The baseband signal is spread using $PN_{\mathrm{WF},1}$ with a chip rate of 93.75 Mcs and translated to a 750-MHz carrier signal with −23.5 dBm output power, serving as the TX SI at the RX input. Fig. 21 shows the baseband RX output when the LO in the RX is code-modulated with code PN_X and $PN_{\mathrm{WF},2}$. As expected from (14) and Fig. 8, despreading the TX SI with PN_X results in a spread baseband SI spectrum at RX output. However, as noted in Section III-C and (14), despreading with $PN_{\mathrm{WF},2}$

TABLE I
PERFORMANCE COMPARED WITH STATE OF THE ART

	This Work	Yang [14], JSSC 15	Zhou [25], JSSC 15	Broek [26], JSSC 15	Zhou [13], ISSCC 16
f_c (GHz)	0.3-1.4	0.5-1.5	0.8-1.4	.15-3.5	0.6-0.8
Arch.	Code-domain N-path Mixer	Mixer-First TX/RX	Wideband SIC†	Mixer First VM SI	Circulator +BB SIC
No. of RX O/P	2	1	1	1	1
RX Gain (dB)	35/38	53	27-42	24	42
RX NF (dB)	2.5-4 + *0.9dB Filter mismatch	5-8	4.8	6.3	5.0
SIRC NF Degradation(dB)	0.9 due to filter mismatch	-	0.9/1.3	4-6	5.9*
IB IIP3 (dBm)	-26	-38.7	-20	+9/+19	-33
SI P1dB (dB)	-11.8	-9.7**	-7.7**	9.3**	-27.7**
SIRC (dB)	38.5	33	25	27	42
BW (MHz)	1	0.6	20	16.25	12*
Power (mW)	LNA: 25.5 LO: 9.5◇ code mod.: ∼1 (sim)	43-56 (incl. TX BB)	107-250 †	23 - 56	160 *
Area (mm^2)	0.31‡	1.5	4.8	2	1.4

*includes N-path circulator antenna interface; NF degraded by LO PN, **computed from measured IIP3 (this work measured integrated power). † Includes filters to cancel across 9ns of peak delay in antenna interface; power consumption scales with one or two filters enabled. ◇ does not include power required for LO synchronization for code domain filtering. ‡ includes area of N-path receiver, IF stages, output buffers and four phase LO generation as shown in Fig. 13.

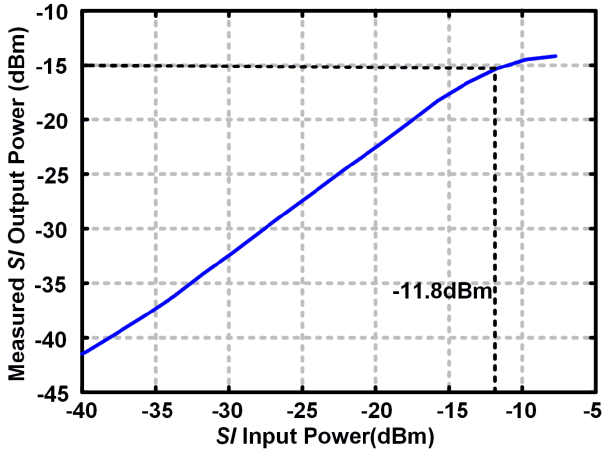

Fig. 22. Measured integrated in-band SI output power for 1.46-Mb/s QPSK SI spread with $PN_{WF,1}$ and despread with $PN_{WF,2}$.

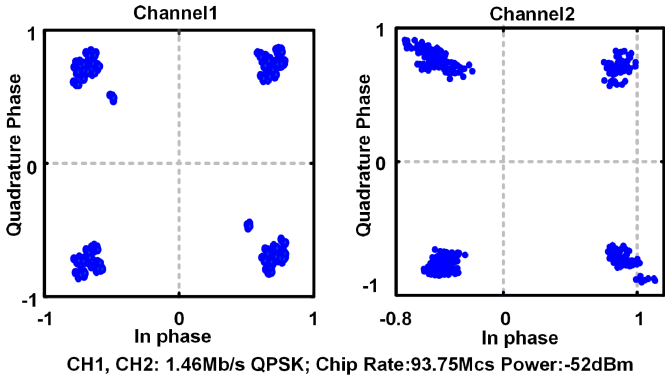

Fig. 23. Concurrent reception of two code-modulated signals using separate codes on the two RX channels at 750 MHz.

results in frequency translation of the SI at the baseband output (7). As shown in Fig. 21 and predicted by (14), the two-tone TX SI is frequency translated to 46.9 MHz, which represents half the 93.75-Mcs chip rate. Importantly, the in-band SI residue is reduced compared with the case for LO modulated with PN_X. The frequency translation of the TX SI out of the RX band enables subsequent frequency filtering to remove SI.

Fig. 22 plots integrated in-band SI power at RX output over 1-MHz integration bandwidth for a 1.46-Mb/s QPSK SI that has been spread using $PN_{\mathrm{WF},1}$ and despread using $PN_{\mathrm{WF},2}$. From Fig. 22, the RX gain with respect to TX SI at RX input is −3 dB. Since the receiver provides 35.5-dB gain for the desired signal, this implies an in-band SI rejection of 38.5 dB from Fig. 22.

Measurements demonstrate −11.8 dBm input-referred P_{1dB} with respect to SI that translates to a +23.7-dBm OP_{1dB} with respect to SI for the RX. This paper does not assume a particular antenna interface in the STAR system. Typically, TX to RX isolation in STAR systems is achieved using duplexers, circulators, or separate antennas for TX and RX. Any isolation provided by the TX/RX antenna interface will be additive to the SI rejection achieved using the proposed technique. For example, if the antenna interface provides 25-dB isolation between TX and RX, the overall isolation would be improved from 38.5 to 63.5 dB. Additionally, the measured −11.8 dBm input-referred P_{1dB} for the SI is referred to the RX input. Therefore, 25-dB TX-to-RX isolation in the antenna interface would imply that a TX output power of 13.2 dBm is supported by this implementation.

C. Measured RX Constellation

Fig. 23 shows the measured constellation for two concurrent QPSK modulated signals with data rate 1.46 Mb/s at 750 MHz, which is spread with different PN codes at chip rate 93.75 Mcs demonstrating concurrent reception. The minimum input power used at antenna is limited by RX gain and input-referred noise of the oscilloscope. Fig. 24

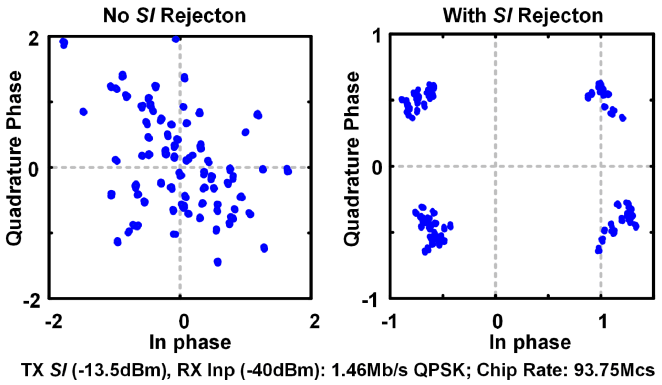

Fig. 24. Reception of the desired 750-MHz signal spread using $PN_{\mathrm{WF},2}$ in the presence of in-band SI spread using $PN_{\mathrm{WF},1}$.

shows receiver constellation recovery with and without SI rejection for −40 dBm desired input and −13.5 dBm SI (both at 1.46-Mb/s QPSK). Constellation recovery following SI rejection demonstrates the feasibility of code-domain STAR operation using N-path RX.

Table I compares the proposed code domain approach with the existing blocker-tolerant RX. This paper extends the use of N-path RX for blocker tolerance and SI rejection/cancellation (SIRC) in the code domain achieving low power consumption and NF degradation with a small area penalty.

VI. Conclusion

Code-modulated LO signals in an N-path RX can be used to achieve code-domain reception of desired signals and rejection of interferers. Modulating known interferers and desired signals with specific pairs of codes provides increased interferer rejection. The blocker tolerance achieved in this paper can be improved upon by using N-path passive-mixer first architectures with code-modulated LO signals. Additionally, other codes that trade OFF cross correlation and synchronization/autocorrelation can be leveraged for system-level optimization. The correlator-based perspective of N-path filters can be further generalized by using orthogonal sequences that are not NOPs as LO signals. Such N-path sequence-mixing filters can demonstrate rejection/reception of signals based on a combination of their code-domain, spectral-domain, and sequence-domain properties.

Acknowledgment

The authors would like to thank Dr. R. T. Olsson, Dr. B. Epstein (DARPA), and Dr. J. Rockway (SPAWAR) for valuable feedback. They would also like to thank R. Fetche and Rohde and Schwarz as well as Tektronix for assistance with test equipment.

References

[1] J. G. Andrews *et al.*, "What will 5G be?" *IEEE J. Sel. Areas Commun.*, vol. 32, no. 6, pp. 1065–1082, Jun. 2014.

[2] A. Sabharwal, P. Schniter, D. Guo, D. W. Bliss, S. Rangarajan, and R. Wichman, "In-band full-duplex wireless: Challenges and opportunities," *IEEE J. Sel. Areas Commun.*, vol. 32, no. 9, pp. 1637–1652, Sep. 2014.

[3] C. Andrews and A. C. Molnar, "Implications of passive mixer transparency for impedance matching and noise figure in passive mixer-first receivers," *IEEE Trans. Circuits Syst. I, Reg. Papers*, vol. 57, no. 12, pp. 3092–3103, Dec. 2010.

[4] A. Ghaffari, E. A. M. Klumperink, M. C. M. Soer, and B. Nauta, "Tunable high-Q N-path band-pass filters: Modeling and verification," *IEEE J. Solid-State Circuits*, vol. 46, no. 5, pp. 998–1010, May 2011.

[5] A. Ghaffari, E. A. M. Klumperink, and B. Nauta, "Tunable N-path notch filters for blocker suppression: Modeling and verification," *IEEE J. Solid-State Circuits*, vol. 48, no. 6, pp. 1370–1382, Jun. 2013.

[6] M. Darvishi, R. van der Zee, E. A. Klumperink, and B. Nauta, "Widely tunable 4th order switched G_m-C band-pass filter based on N-path filters," *IEEE J. Solid-State Circuits*, vol. 47, no. 12, pp. 3105–3119, Dec. 2012.

[7] C.-K. Luo, P. S. Gudem, and J. F. Buckwalter, "A 0.2–3.6-GHz 10-dBm B1 dB 29-dBm IIP3 tunable filter for transmit leakage suppression in SAW-less 3G/4G FDD receivers," *IEEE Trans. Microw. Theory Techn.*, vol. 63, no. 10, pp. 3514–3524, Oct. 2015.

[8] Y. Lien, E. Klumperink, B. Tenbroek, J. Strange, and B. Nauta, "A high-linearity CMOS receiver achieving +44 dBm IIP3 and +13 dBm B1 dB for SAW-less LTE radio," in *IEEE Int. Solid-State Circuits Conf. (ISSCC) Dig. Tech. Papers*, Feb. 2017, pp. 412–413.

[9] A. Ghaffari, E. A. M. Klumperink, F. van Vliet, and B. Nauta, "A 4-element phased-array system with simultaneous spatial- and frequency-domain filtering at the antenna inputs," *IEEE J. Solid-State Circuits*, vol. 49, no. 6, pp. 1303–1316, Jun. 2014.

[10] L. Zhang, A. Natarajan, and H. Krishnaswamy, "Scalable spatial notch suppression in spatio-spectral-filtering MIMO receiver arrays for digital beamforming," *IEEE J. Solid-State Circuits*, vol. 51, no. 12, pp. 3152–3166, Dec. 2016.

[11] A. Agrawal and A. Natarajan, "A concurrent dual-frequency/angle-of-incidence spatio-spectral notch filter using walsh function passive sequence mixers," in *IEEE MTT-S Int. Microw. Symp. Dig.*, Jun. 2017, pp. 1606–1609.

[12] N. Reiskarimian, J. Zhou, and H. Krishnaswamy, "A CMOS passive LPTV nonmagnetic circulator and its application in a full-duplex receiver," *IEEE J. Solid-State Circuits*, vol. 52, no. 5, pp. 1358–1372, May 2017.

[13] J. Zhou, N. Reiskarimian, and H. Krishnaswamy, "Receiver with integrated magnetic-free N-path-filter-based non-reciprocal circulator and baseband self-interference cancellation for full-duplex wireless," in *IEEE Int. Solid-State Circuits Conf. (ISSCC) Dig. Tech. Papers*, Jan. 2016, pp. 178–180.

[14] D. Yang, H. Yüksel, and A. Molnar, "A wideband highly integrated and widely tunable transceiver for in-band full-duplex communication," *IEEE J. Solid-State Circuits*, vol. 50, no. 5, pp. 1189–1202, May 2015.

[15] A. Agrawal and A. Natarajan, "A 0.3 GHz to 1.4 GHz N-path mixer-based code-domain RX with TX self-interference rejection," in *Proc. IEEE Radio Freq. Integr. Circuits (RFIC) Symp.*, Jun. 2017, pp. 272–275.

[16] D. Bharadia, E. McMilin, and S. Katti, "Full duplex radios," in *Proc. ACM SIGCOMM Conf.*, 2013, pp. 375–386.

[17] C. Andrews, C. Lee, and A. Molnar, "Effects of LO harmonics and overlap shunting on N-phase passive mixer based receivers," in *Proc. Eur. Solid-State Circuits Conf. (ESSCIRC).*, Sep. 2012, pp. 117–120.

[18] A. Goldsmith, *Wireless Communications*. Cambridge, U.K.: Cambridge Univ. Press, 2005.

[19] J. G. Proakis and M. Salehi, *Fundamentals Communication Systems*. London, U.K.: Pearson, 2007.

[20] R. Gold, "Maximal recursive sequences with 3-valued recursive cross-correlation functions (Corresp.)," *IEEE Trans. Inf. Theory*, vol. 14, no. 1, pp. 154–156, Jan. 1968.

[21] T. Kasami, "Weight distribution formula for some class of cyclic codes," Coordinated Sci. Lab., Urbana, IL, USA, Tech. Rep. R-285, 1966.

[22] H. F. Harmuth, "Applications of Walsh functions in communications," *IEEE Spectr.*, vol. 6, no. 11, pp. 82–91, Nov. 1969.

[23] D. Pozar, *Microwave Engineering*. Hoboken, NJ, USA: Wiley, 2004.

[24] Z. Lin, P.-L. Mak, and R. P. Martins, "A 0.028 mm^2 11 mW single-mixing blocker-tolerant receiver with double-RF N-path filtering, S11 centering, +13 dBm OB-IIP3 and 1.5-to-2.9 dB NF," in *IEEE Int. Solid-State Circuits Conf. (ISSCC) Dig. Tech. Papers*, Feb. 2015, pp. 1–3.

[25] J. Zhou, T.-H. Chuang, T. Dinc, and H. Krishnaswamy, "Integrated wideband self-interference cancellation in the RF domain for FDD and full-duplex wireless," *IEEE J. Solid-State Circuits*, vol. 50, no. 12, pp. 3015–3031, Dec. 2015.

[26] D.-J. van den Broek, E. A. M. Klumperink, and B. Nauta, "An in-band full-duplex radio receiver with a passive vector modulator downmixer for self-interference cancellation," *IEEE J. Solid-State Circuits*, vol. 50, no. 12, pp. 3003–3014, Dec. 2015.

Abhishek Agrawal (M'14) received the B.Tech. degree in engineering physics from the Indian Institute of Technology Madras, Chennai, India, in 2008, and the Ph.D. degree in electrical engineering from Oregon State University, Corvallis, OR, USA, in 2017.

He is currently a Research Scientist with Intel Corporation, Hillsboro, OR, USA. His current research interests include the design of RF and mm-wave transmitters and receivers in CMOS as well as phased-array and MIMO circuits and systems.

Dr. Agrawal was a recipient of the Analog Devices Outstanding Student Designer Award in 2016.

Arun Natarajan (M'02) received the B.Tech. degree in electrical engineering from the Indian Institute of Technology Madras, Chennai, India, in 2001, and the M.S. and Ph.D. degrees in electrical engineering from the California Institute of Technology, Pasadena, CA, USA, in 2003 and 2007, respectively.

From 2007 to 2012, he was a Research Staff Member with the IBM T. J. Watson Research Center, Yorktown Heights, NY, USA, where he was involved in millimeter-wave (mm-wave) phased arrays for multi-Gb/s data links and airborne radar and on self-healing circuits for increased yield in submicrometer process technologies. In 2012, he joined Oregon State University, Corvallis, OR, USA, as an Assistant Professor with the School of Electrical Engineering and Computer Science. His current research interests include RF, mm-wave, and sub-mm-wave integrated circuits and systems for high-speed wireless communication and imaging.

Dr. Natarajan was a recipient of the National Talent Search Scholarship from the Government of India [1995–2000], the Caltech Atwood Fellowship in 2001, the IBM Research Fellowship in 2005, the 2011 Pat Goldberg Memorial Award for the Best Paper in computer science, electrical engineering, and mathematics published by IBM Research, the CDADIC Best Faculty Project Award in 2014 and 2016, the NSF CAREER Award in 2016, and the Oregon State University Engelbrecht Young Faculty Award in 2016. He serves on the Technical Program Committee of the IEEE International Solid-State Circuits Conference and the IEEE Radio-Frequency Integrated Circuits Conference. He is an Associate Editor of the IEEE TRANSACTIONS ON VERY LARGE SCALE INTEGRATION SYSTEMS and the IEEE TRANSACTIONS OF MICROWAVE THEORY AND TECHNIQUES.